BAR-SUPPORTED AND UNSUPPORTED DENTAL IMPLANTS: A QCT-FEA STUDY IN HUMAN MAXILLA

Luboš Řehounek*, Aleš Jíra

Czech Technical University in Prague, Faculty of Civil Engineering, Department of Mechanics, Thákurova 7, 166 29 Prague 6, Czech Republic

* corresponding author: `lubos.rehounek@fsv.cvut.cz`

Abstract. Two variants of implant-supported overdentures (IODs) were investigated by quantitative computed tomography-assisted finite element method (QCT-FEA) on a patient-specific CT-reconstructed model of human maxilla. The analyzed variants are bar-supported (splinted) and unsupported (unsplinted) implant assemblies. The loading was done by a $800\,\mathrm{N}$ force slanted by $30°$ in the buccolingual direction. The results of the analyses show favorable stress distributions for the bar-supported variant.

Keywords: Bar-supported, dental, implant, stress, maxilla.

1. Introduction

The main purpose of FEM (Finite Element Method) is the reduction of a complex problem into a set of algebraic equations to help better understand the problem or predict its behavior. In the biomedical field, use of FEM is both particularly useful and hard to do, as the problems are usually very difficult to describe by a simple model and boundary conditions and material properties are often subjects of long studies, complex methods or simply making an educated guess. Therefore, use of QCT-FEA by clinical practitioners can be both beneficial (insight into the patient's conditions) and virtually impossible (integration into clinical practice) [1]. However, QCT-FEA is still the only reliable method of estimating the bone's mechanical properties for patients as no contemporary in vivo method is able to do it. This leaves us with the need to assess its usability in real clinical practice. One of such examples of its use can be the example of bar-supported (or bar-retained) and unsupported dentures.

A very popular means of treating edentulism (loss of all teeth) is to prepare the patient's jaw for placement of 4 load-bearing dental implants that carry an overdenture [2]. These implants can either be unsupported – placed individually with no structural connections, or supported – usually with a soldered metal wire or a solid bar that acts as a stirrup that connects all 4 implants together for better distribution of masticatory forces. The former option is the standard in dental practice as it requires less customization and is less time intensive. However, the bar-supported variant finds its use if the patient's bone quality is poor, implants are located in the maxilla (upper jaw) or the implants are divergent and additional support is needed to maintain their proper position [3]. Moreover, bar-supported (or bar-retained) implant-supported overdentures (IODs) have a survival rate of ca. $97\,\%$ in a period >7 years post-operation as reported by authors [4–7].

Another great benefit of the bar-supported system is anti-rotational stability, as reported by [8–10]. Bar-supported IODs also provide the advantages of both removable and fixed prostheses as they require low maintenance and provide good stability [11]. Another benefit of bar-supported IODs is the fact that they are not correlated with any significant plaque accumulation, bone loss, peri-implantitis or other adverse conditions [12].

Studies also suggest that placing an overdenture in the mandible (lower jaw) provides excellent long-term stability and positive outcomes, but when they are used in the maxilla, outcomes are less favorable [13], hence the need for bar-supported variants. For the mandible, use of two or four splinted implants is a feasible option as bars are not necessary [14]. The QCT-FEA reconstruction is shown on Figure 1.

2. Materials and Methods

This work analyzes differences in stress distributions of both variants (unsupported and bar-supported). For that purpose, the QCT-FEA (Quantitative Computed Tomography-Based Finite Element Analysis) method was used. The QCT-FEA method uses patient-specific CT scans calibrated using a Phantom device so that every pixel is assigned a unique value of the Hounsfield unit (sometimes referred to as the Hounsfield number in CT imaging) for every pixel in every image slice so that the final reconstructed model has specific values for every voxel. The readings correspond to the amount of light reflected back by the material during scanning. The Hounsfield Unit Scale (HU) values are computed according to this equation:

$$HU = 1000 \times \frac{\mu_{\mathrm{tissue}} - \mu_{\mathrm{water}}}{\mu_{\mathrm{water}} - \mu_{\mathrm{air}}}, \qquad (1)$$

where the value of water μ_{water} is arbitrarily assigned as $0\,\mathrm{HU}$, $\mu_{\mathrm{air}} = -1000\,\mathrm{HU}$ and all other values are calculated [15].
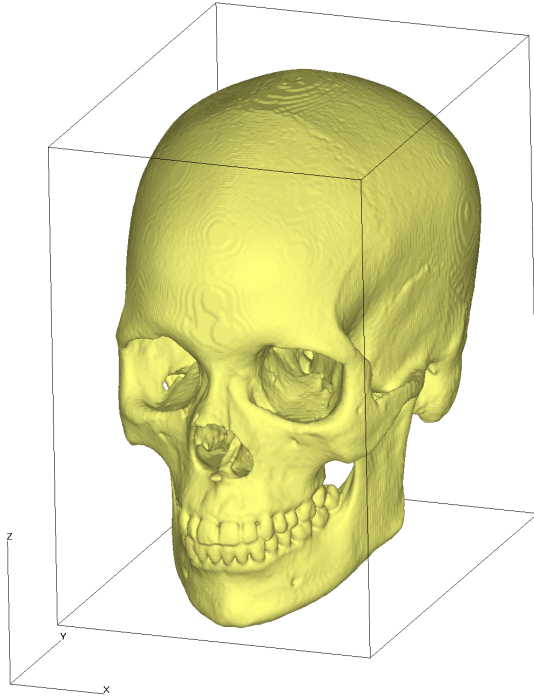
FIGURE 1. Render of the patient-specific model that was used for numerical simulations. The maxilla and surrounding bone tissue was extracted from this model, as shown on Figure 2. Note that CT data often contains a lot of noise or unwanted elements out of the desired threshold range, so preparation of the patient-specific CT data for QCT-FEA up to this point can take anywhere between minutes and hours based on the size of the specimen.

The program used was Mechanical Finder. It is a QCT-FEA software that fully utilizes the Hounsfield unit conversion into a fully inhomogeneous material model (inhomogeneity on Figure 2) for bone based on the readings from the patient-specific CT scan and using a material conversion equation. This equation is provided by Keyak [16]:

$$\rho \ [\mathrm{mgcm^{-3}}] = \text{CT value [HU]} \times a + b, \qquad (2)$$

where ρ is material density and $\rho \geq 0$. Parameters a and b are determined for each voxel by the calibration phantom (a set of rods of known densities).

The numerical model consists of the patient-specific 3D bone model of human maxilla and of an imported .STL implant part. The implant assembly was modelled in 2 variants – bar-supported and without bars. The program used to create the models was ANSYS Spaceclaim. Position of the implants, their shape and location was modelled according to data provided by an anonymous patient. The analyzed implant variants can be seen on Figure 3.

The mesh of the model was created with respect to the details of the implants. Also, shell elements were created on the surface of the bone material as cortical bone is usually too thin to be represented with a single element and there is a concern for accuracy [17].
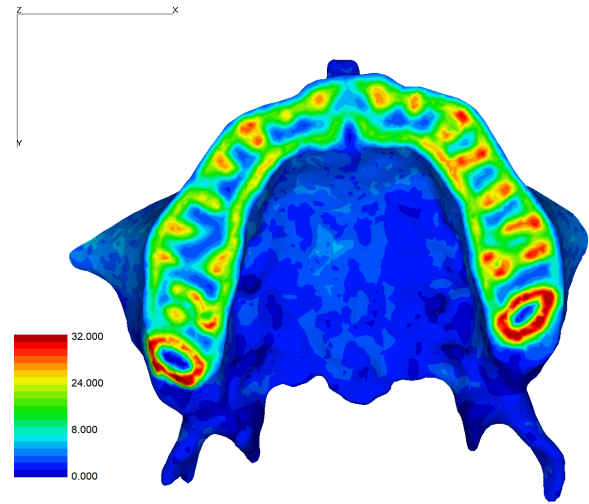

FIGURE 2. Map of Young's modulus E [GPa] that on the QCT-FEA model of a human maxilla. Image shows an arbitrary transversal section of the maxilla that was obtained by a phantom-calibrated patient-specific CT scan.
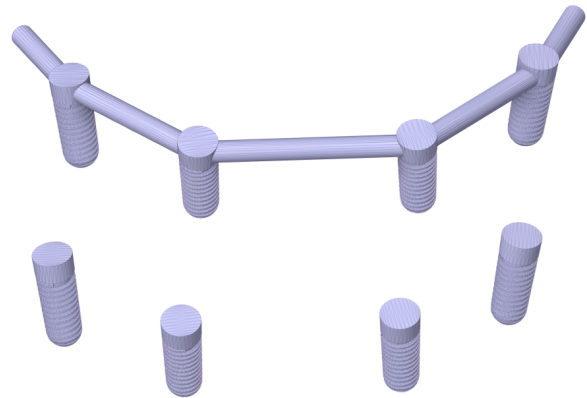

FIGURE 3. Two analyzed variants of the implant assembly.Top – the bar-supported variant, bottom – only intraosseous implants.

The two variants were analyzed under the same exact conditions in regard to placement of the intraosseous implants, their material properties (Ti-6Al-4V alloy with Von-Mises yield criterion) and bone properties and geometry. The models with boundary conditions can be seen on Figure 4.

The analysis was performed as fully non-linear in terms of material and geometry. The analysis was divided into 10 substeps so that every increment adds 80 kN of load. The deformations of the models can be seen in detail in Figure 5.

Both simulations were performed using a personal computer with 64 GB of RAM and a 16-thread 4.7 GHz processor. Both computations were completed under 1 minute – an important factor for real time use by physicians, as will be discussed.

3. RESULTS

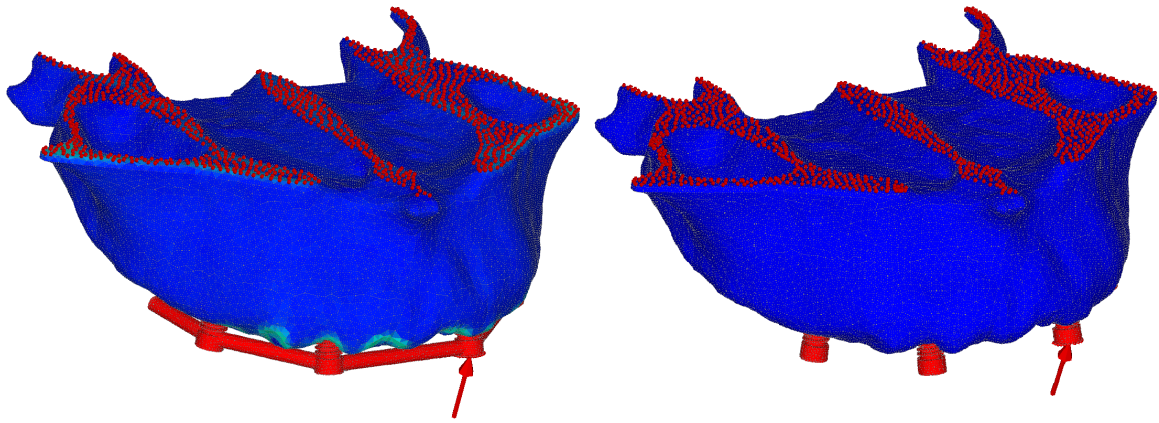The results shown on Figure 5 show the gradual deformation of both variants in various times. As we

FIGURE 4. Both configurations of the analysis with boundary conditions. Geometry of bone material and the position of the implant assembly is identical. The only difference are the supporting bars on the first variant. The model is an extracted part of an anonymized CT scan of a human skull presented on Figure 1. The part was extracted and fixed on the upper surface. A 30° slanted 800 N force was applied on the surface of the third implant from the left.
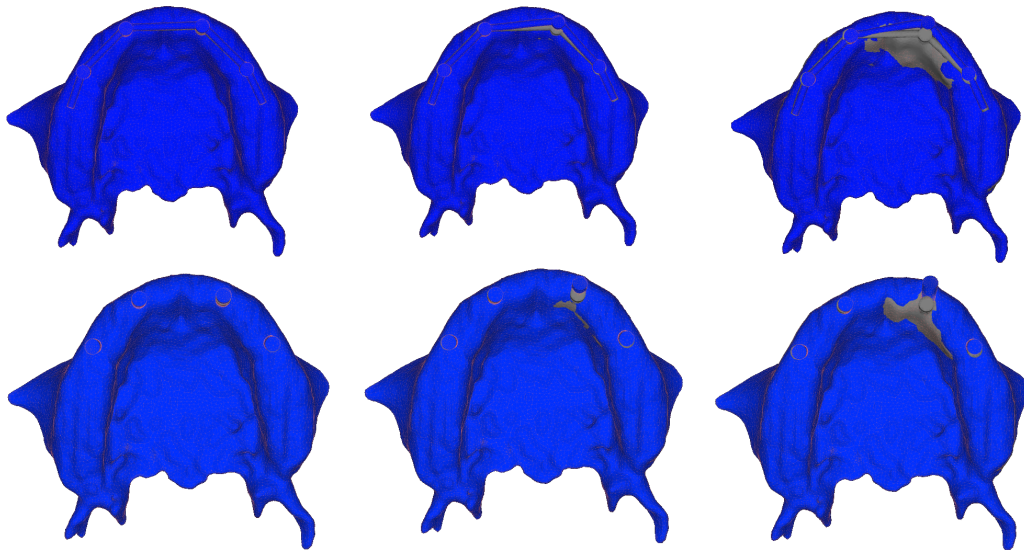

FIGURE 5. Changes in geometry of the two modelled variants during the simulation. Top row – bar-supported variant, bottom row – unsupported variant. The loads at which the deformations were captured are, beginning from left: $F = 80$ N, $F = 400$ N, $F = 800$ N (corresponding steps 1, 5 and 10, respectively). Gray color represents the original, undeformed geometry and blue color represents the deformed state. Deformations are magnified $50\times$.

can see, the different deformation of the implant is accentuated in the final substep of the analysis. The bar-supported variant shows smaller displacements of the implant that is loaded thanks to the additional stiffness provided by the connections to other implants.

The main analyzed quantity was stress risk factor in bone. As we can see from overviews on Figure 6, the inclusion of the bar changes the distribution of stress (but mainly its values). Specifically, the risk factor is calculated simply as:

$$RF = \frac{\text{Max. Principal Stress [MPa]}}{\text{Critical Stress [MPa]}} \ [\%], \quad (3)$$

where critical stress is assigned by conversions provided by [16].

4. CONCLUSIONS

The QCT-FEA analyses of the interaction of bone and two variants of the implant assembly (bar-supported and unsupported, Figure 4) showed a predictable outcome favoring the bar-supported variant. This is illustrated on Figure 6 and also on Figure 7 for the implant assemblies. However, this does not mean that bar-supported variants are always better in clinical practice as the decision-making process involves many other factors (patient specific conditions like bone quality, necessity of installation of bars, time demands or financial situation of the patient). The results are in agreement with another study on similar topics [18].

Another factor worth discussing is the usability of QCT-FEA simulations for real-time decisions of clinical practitioners on-site. Contemporary level of
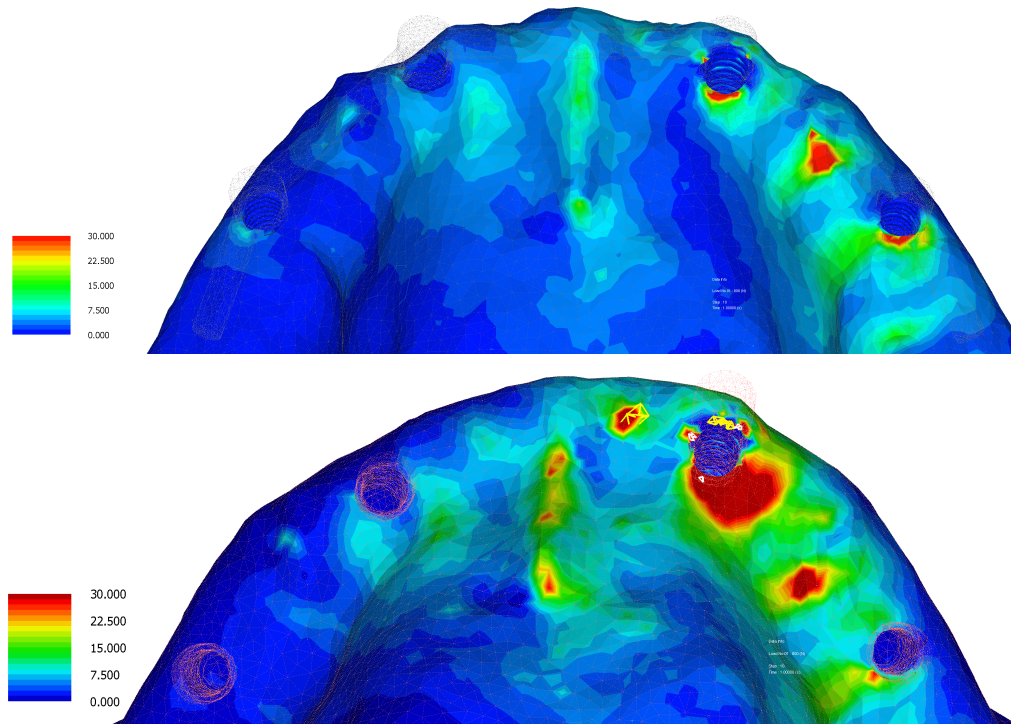
FIGURE 6. Risk factor (RF, Equation (3)) of both variants of the assembly at the final computation step ($F = 800\,\mathrm{N}$). The first image shows the bar-supported variant, where stresses are better distributed and there are no cracked, crushed or plastic solid elements. The unsupported variants shows much larger pools of concentrations of stress and also some plastic elements (yellow boxes) and cracked elements (white lines). The scale for RF was chosen in the range of 0–30 % to better illustrate the stress distribution in the bone as the scale of 0–100 % would leave the reader oblivious to the small areas. Deformations magnified 50×.
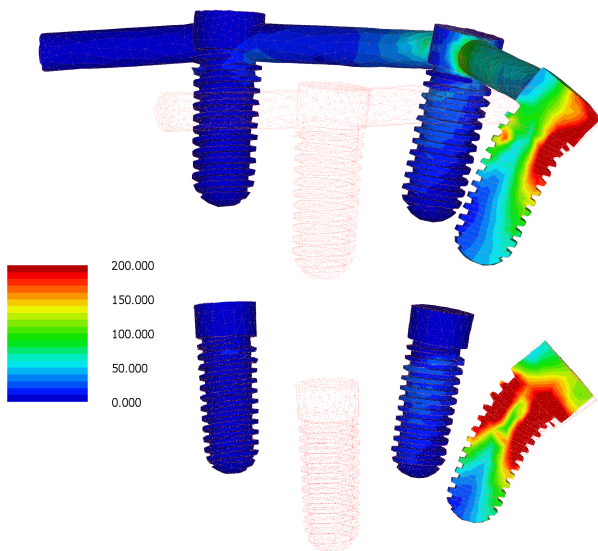

FIGURE 7. Von-Mises stress [MPa] displayed on a sagittal section of the implant assemblies. The bar-supported variant shows better stress distribution with the help of the bars. Deformations magnified 50×.

complexity, price availability and the time-consuming process of analysis of most QCT-FEA software does not allow for on-site patient-specific simulations directly by clinical practitioners. However, it similar tools are refined and practitioners are led to understand inputs and outputs of FEA, it might be possible to have some level of involvement in the future. This involvement would mainly include deciding between multiple implant types the practitioner has at their disposal, evaluating the quality of bone via CT scan analyses and deciding on the needs and/or risks of operation. The simulations of presented study took less than 1 minute to complete each – a time short enough to perform on-site. However, the expertise needed to operate QCT-FEA software, its hard introduction en masse among practitioners and the need to perform phantom-calibrated CT scans beforehand limit its use as a practical everyday tool today. This hinderance begs the question whether one might be better off without the need for a phantom device.

There are also other algorithms for prediction of mechanical properties of bone without the need for a phantom device as suggested by Prado [19]. Their ease of operability as compared to having a phantom device, which might be more difficult to get, but much more easy to work with and more precise once available, seem to be the step in the right direction. Their evaluation, however, remains a topic for further research.

References

[1] K. Engelke, B. van Rietbergen, P. Zysset. FEA to measure bone strength: a review. *Clinical reviews in bone and mineral metabolism* **14**(1):26–37, 2016. https://doi.org/10.1007/s12018-015-9201-1

[2] M. Taruna, B. Chittaranjan, N. Sudheer, et al. Prosthodontic perspective to All-on-4® concept for dental implants. *Journal of clinical and diagnostic research: JCDR* **8**(10):ZE16, 2014. https://doi.org/10.7860/jcdr/2014/9648.5020

[3] L. Vega, R. Strait, T. E. Ames. Bar-retained zygomatic implant overdenture as a first line of treatment. *Compendium* **43**(7), 2022.

[4] S. Rinke, H. Rasing, N. Gersdorff, et al. Implant-supported overdentures with different bar designs: A retrospective evaluation after 5-19 years of clinical function. *The journal of advanced prosthodontics* **7**(4):338–343, 2015. https://doi.org/10.4047/jap.2015.7.4.338

[5] G. Krennmair, M. Krainhöfner, E. Piehslinger. The influence of bar design (round versus milled bar) on prosthodontic maintenance of mandibular overdentures supported by 4 implants: a 5-year prospective study. *International Journal of Prosthodontics* **21**(6):514–520, 2008.

[6] G. Krennmair, E. Piehslinger. Removable implant-supported maxillary prostheses anchored on milled bars: a retrospective evaluation of two concepts. *International Journal of Prosthodontics* **22**(6):576–578, 2009.

[7] M. Andreiotelli, W. Att, J.-R. Strub. Prosthodontic complications with implant overdentures: a systematic literature review. *International Journal of Prosthodontics* **23**(3):195–203, 2010.

[8] G. Krennmair, D. Sütö, R. Seemann, E. Piehslinger. Removable four implant-supported mandibular overdentures rigidly retained with telescopic crowns or milled bars: a 3-year prospective study. *Clinical oral implants research* **23**(4):481–488, 2012. https://doi.org/10.1111/j.1600-0501.2011.02169.x

[9] L. Tang, J. P. Lund, R. Tache, et al. A within-subject comparison of mandibular long-bar and hybrid implant-supported prostheses: psychometric evaluation and patient preference. *Journal of dental research* **76**(10):1675–1683, 1997. https://doi.org/10.1177/002203459707601009

[10] S. J. Sadowsky. Mandibular implant-retained overdentures: A literature review. *The Journal of prosthetic dentistry* **86**(5):468–473, 2001. https://doi.org/10.1067/mpr.2001.119921

[11] G. Krennmair, M. Krainhöfner, E. Piehslinger. Implant-supported mandibular overdentures retained with a milled bar: a retrospective study. *International Journal of Oral & Maxillofacial Implants* **22**(6):987–994, 2007.

[12] K. M. Lehmann, P. W. Kämmerer, J. Karbach, et al. Long-term effect of overdenture bar design on peri-implant tissues. *The International Journal of Oral & Maxillofacial Implants* **28**(4):1126–1131, 2013. https://doi.org/10.11607/jomi.2161

[13] C. Mangano, F. Mangano, J. A. Shibli, et al. Morse taper connection implants supporting "planned" maxillary and mandibular bar-retained overdentures: a 5-year prospective multicenter study. *Clinical Oral Implants Research* **22**(10):1117–1124, 2011. https://doi.org/10.1111/j.1600-0501.2010.02079.x

[14] I. Naert, G. Alsaadi, D. van Steenberghe, M. Quirynen. A 10-year randomized clinical trial on the influence of splinted and unsplinted oral implants retaining mandibular overdentures: peri-implant outcome. *International Journal of Oral & Maxillofacial Implants* **19**(5), 2004.

[15] D. R. Dance, S. Christofides, A. D. A. Maidment, et al. (eds.). *Diagnostic radiology physics: A handbook for teachers and students.* International Atomic Energy Agency, Vienna, 2014.

[16] J. H. Keyak, S. A. Rossi, K. A. Jones, H. B. Skinner. Prediction of femoral fracture load using automated finite element modeling. *Journal of biomechanics* **31**(2):125–133, 1997. https://doi.org/10.1016/S0021-9290(97)00123-1

[17] A. Mendizabal Dones. *Finite Element Simulation: Tensile test of rib cortical bone.* Master's thesis, Chalmers University of Technology, 2010.

[18] Ö. Kümbüloğlu, B. Koyuncu, G. Yerlioğlu, et al. Stress distribution on various implant-retained bar overdentures. *Materials* **15**(9):3248, 2022. https://doi.org/10.3390/ma15093248

[19] M. Prado, S. Khosla, C. Chaput, H. Giambini. Opportunistic application of phantom-less calibration methods for fracture risk prediction using QCT/FEA. *European radiology* **31**(12):9428–9435, 2021. https://doi.org/10.1007/s00330-021-08071-w